Seabed Stresses in Combined Wave and Steady Flow Conditions on the Nova Scotia Continental Shelf: Field Measurements and Predictions

D. A. HUNTLEY AND D. G. HAZEN

Department of Oceanography, Dalhousie University, Halifax, Nova Scotia, Canada

(Manuscript received 8 May 1986, in final form 31 July 1987)

ABSTRACT

A tripod holding electromagnetic flowmeters at two heights within 1 m above the seabed has been deployed at two shallow sites (25 and 45 m depths) on the continental shelf off Nova Scotia, Canada. Wave flows are comparable with the small mean flows at both sites. Friction velocities have been estimated from the observed spectra of vertical turbulent velocities, using a modification of the dissipation method appropriate to low Reynolds number conditions. The results from each site show no significant change of friction velocity with height, as expected for measurements from within the constant stress layer. However, in each case the observed friction velocities are considerably larger than would be predicted on the basis of the observed bottom roughness and the mean flows alone, indicating that the wave flows were important in enhancing the friction velocity. The theory of Grant and Madsen (1979) has been used to predict the friction velocities, based on the observed mean and wave velocities and on the bottom roughness estimated from stereophotography of the seabed. Good agreement is found between the predicted and observed friction velocities at both sites provided that the significant orbital velocity amplitude is used in the predictions. This is in general agreement with the results of Grant et al.

1. Introduction

Near bottom wave-induced currents are likely to be significant over most of the continental shelf, particularly during storms. Butman et al. (1979), for example, show that sediment movement by waves can occur right out to the edge of the shelf. We might expect on theoretical grounds that waves of period 5–15 s will start to "feel" the seabed in about 20–180 m water depth respectively. Therefore, it is somewhat surprising that, until recently, little attention has been paid to seabed stresses under conditions of combined wave and mean currents. Initial theoretical investigations centered around finding a formula that would give the correct form in the opposite limits of no waves or no currents (for example, see Jonsson, 1966). More recently two rather similar nonlinear theories of wave and current boundary layers have been proposed, by Smith (1977) and by Grant and Madsen (1979).

These two nonlinear theories are based on different assumptions about the variation of the turbulent eddy viscosity with height above the bed, but both predict substantially increased bottom stresses and apparent bottom roughnesses when waves are superimposed on a mean flow. Since such increased bottom stresses are significant for models of low-frequency flows on the continental shelf (e.g., Clarke and Brink, 1985) and also for sediment transport (e.g., Larsen et al., 1981), it is important to test the predictions of these theories with field data.

Recent measurements from continental shelf environments provide some support for the nonlinear theories of enhanced bottom friction. Grant and Madsen (1986) review these measurements. Wiberg and Smith (1983) reanalyze data from the Alaskan Shelf collected by Cacchione and Drake (1982) and find, with suitable adjustment of the sensor heights and a small adjustment to the sensitivity of one sensor, that the measured values of friction velocity u_* [= (bottom stress/water density)$^{1/2}$] are more than twice those predicted for the mean flows alone, but are in fair, though not excellent, agreement with predictions based on both the Smith (1977) and Grant and Madsen (1979) theories. Grant et al. (1984, hereafter GWG) used data from the Coastal Ocean Dynamics Experiment (CODE) on the continental shelf off Northern California to test the Grant and Madsen (1979, hereafter GM) predictions. A bottom mounted tripod held acoustic current sensors at four heights above the bed, to a maximum height of about 2 m. Data from the sensors were used to estimate both turbulent stress and apparent bottom roughness from mean velocity profiles, and stresses alone from the vertical turbulent velocity spectra by using the "inertial dissipation" method. The authors find good (10%–15%) agreement between their observations and the predictions of GM. However, there is some uncertainty about the contribution of bedforms to the large measured stresses (Huntley, 1985; Grant and Williams,

Corresponding author address: Dr. David Huntley, Institute of Marine Studies, Plymouth Polytechnic, Drake Circus, Plymouth, Devon PL4 8AA, United Kingdom.

1985). Gust (1985) also points out two apparent errors in their use of the dissipation method for estimating bottom stress. The GWG results are revised and discussed at length in Huntley (1988).

Thus there is a clear need for further fieldwork to test and possibly extend existing theories for wave/mean flow boundary layers. It is also important, in order to interpret field data adequately, that such fieldwork involves quantitative measurements of seabed topography over as extensive an area as possible, to provide accurate estimates of bottom roughness (Huntley, 1985).

This paper describes field measurements of waves, mean flow and turbulence within 1 m of the seabed at two sites on the Nova Scotia continental shelf. The data are limited in the number of heights at which measurements were made, in the lengths of the datasets, and in the range of wave and mean flow conditions encountered. Nevertheless, the results support the hypothesis that wave influence is important in modifying the stresses felt by a mean flow, and the GM theory is found to provide a reasonable and consistent estimate of the measured stresses.

2. The measurement system

a. Currents

The central component of our measurement system is a tripod 2 m high and 2 m span on which the sensors are mounted. The tripod is constructed of 2-inch (5 cm) diameter aluminum tubing. An additional frame of aluminum channel and angle holds a heated thermistor profiling apparatus, cantilevered out about 2 m from the centerline of the tripod (Fig. 1). Despite this apparently vibration-prone design, the tripod is rigidly constructed to minimize vibrations, and there was no obvious evidence for natural oscillations of the tripod in the data discussed in this paper. Natural oscillation frequencies are in any case much higher than the frequencies discussed here. Marsh–McBirney model 512 electromagnetic (EM) flowmeters are mounted on a vertical stainless-steel rod of 0.5-inch (1.27 cm) diameter held near to the centerline of the tripod. Two EM sensors are mounted at each vertical height, with their axes horizontal but orthogonal to each other, so that each sensor measures the vertical component of velocity and one orthogonal horizontal component. The sensor heads in this configuration are at least four sensor diameters apart, and calibrations in a laboratory towing tank confirm that this is sufficient to ensure independence of the sensors. In the measurements discussed here two or three sensor pairs of this kind were deployed at different heights.

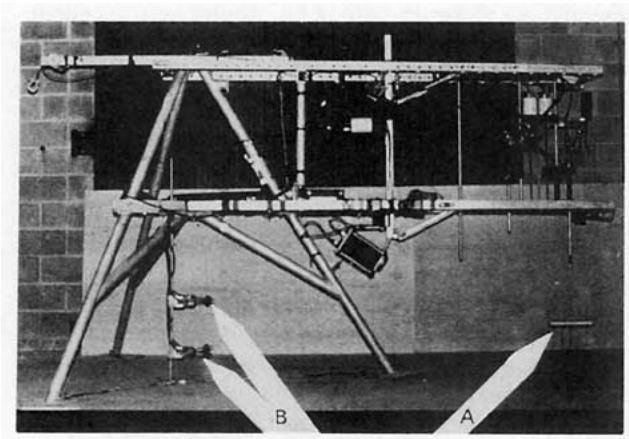

FIG. 1. Photograph of the bottom boundary-layer tripod, showing the configuration of the heated thermistor profiler (A), and the positions of the electromagnetic flowmeter pairs at two levels (B).

The heated thermistor system is similar to that used by Caldwell and Chriss (1979) and Chriss and Caldwell (1982) on the Oregon continental shelf, with the exception that, in the present system, the vertical position of the sensors can be controlled remotely from the ship and the sensors can be either held in position or profiled continuously. Heated thermistor measurements are difficult to interpret in a wave environment, with frequent flow reversals. However, the heated thermistor system was used in one of the two deployments described in this paper, and data from the system has been used to determine the zero-flow offset voltages of the EM sensors.

Other sensors attached to the tripod include a stereo camera, an optical transmissometer, a digital compass, and direction vanes for monitoring mean flow direction. On later deployments, a strain gauge between the tripod and the mooring cable was used to monitor forces between the cable and the tripod.

Figure 2 shows a block diagram of the data acquisition system. Analog signals from the sensors are digitized at the tripod by two 16 channel, 12 bit A/D converters and the digital data are then transmitted by double-armoured electrical cable to a ship maintaining position near the tripod. The double-armoured cable also serves to transmit electrical power to the tripod to drive the sensors and profiler motors. Digital commands from the shipboard control systems are transmitted down the cable to control profiler positions and select the sensor channels to be digitized. The tripod and data acquisition system were described by Chriss et al. (1983).

A "single-point" mooring scheme was used with this tripod, in which the electrical armoured cable went directly from the tripod to a subsurface buoy about half way to the surface, and then looped, under its own weight or with additional chain-link weights, to the surface buoy. For the Sable Island Bank dataset a mooring design program was used to optimize the cable length and placement of subsurface buoyancy to ensure minimum strain on the tripod and minimum transmission of surface motion to the tripod. A strain gauge was placed at the anchor point between the cable and

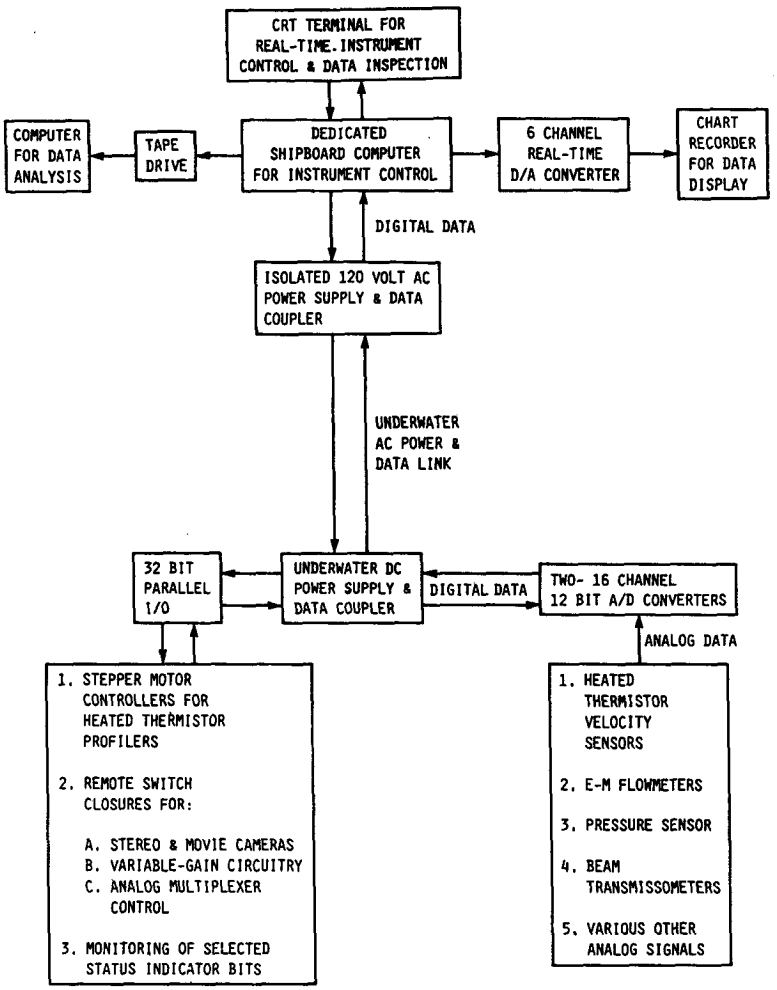

FIG. 2. Block diagram of the data logging system. (Note that pressure sensors and stepper motors were not used in the deployments discussed in this paper.)

the tripod to monitor forces transmitted down the cable.

b. Seabed topography

A stereo camera was attached to the tripod during deployment. However, a single stereophotograph taken from close enough to the bed to resolve accurately the smaller topographic scales (1 m above the bed is a typical camera height) covers only about 0.5 m^2 of the seabed, and therefore has limited ability to measure bedform variability and longer length-scale features. A new Traversing Underwater Photogrammetry System (TUPS) was therefore designed, increasing the continuous stereophotographic coverage of the seabed to about 11 m^2 without degrading the small-scale resolution. The system consists of a frame holding a 6 m long horizontal track, positioned either 1 or 2 m off the seabed, along which a stereo camera is moved by a self-contained, microprocessor-controlled stepper motor system. The resulting mosaic of stereo-pairs can be converted to quantitative measurements of seabed topography by standard photogrammetric techniques. The system has worked well. An example of the output and its relevance to bottom stress prediction will be discussed below.

3. Description of the datasets

The datasets discussed in this paper come from two locations on the Nova Scotia continental shelf, and were collected on two separate cruises (Fig. 3).

In July 1984 the tripod was deployed in 25 m water depth in Cow Bay, Nova Scotia (44°35.63'N, 63°22.85'W). The EM sensors were deployed at 52 and 22 cm above the bed, providing measurements of the horizontal components and two measurements of the vertical component of flow at each level. With the exception of one of the vertical components of the EM sensors at the lower level, all sensors including the

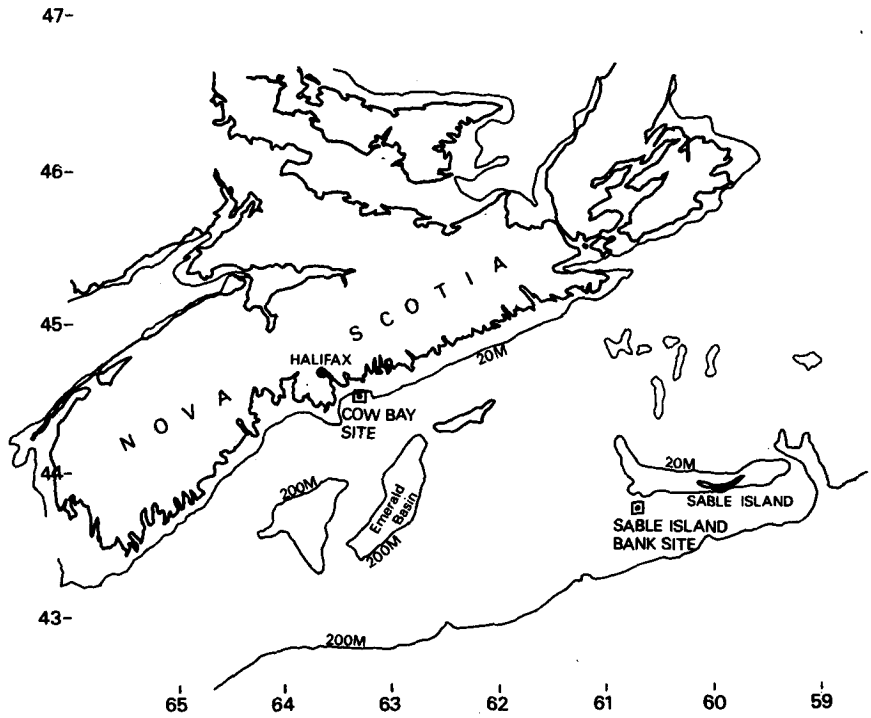

FIG. 3. Map of the Nova Scotia continental shelf, showing the locations of the deployments.

heated thermistors, positioned at a fixed height of 65 cm above the bed, generally performed very well.

The least satisfactory aspect of this dataset is the variability of the bottom roughness at the Cow Bay site. The deployment site was chosen because previous surveys had suggested that it was a region of rippled sandy seabed. However, our first grab sample in the region revealed cobbles of various sizes. Lacking time to move a large distance to a new site, we conducted a grab sample survey over a square about 650 m on a side, about 650 m from the original grab sample site. At each of the corners of this square, sand was recovered in grab samples. The tripod was subsequently deployed as close as possible to this surveyed square but a stereophotograph taken from the tripod after deployment indicates that the actual deployment site was characterized by rounded cobbles ranging in diameter up to 18 cm. More recent surveys reveal the variability of bottom types in this region (Hall, 1985; LaPierre, 1985). We will have to allow for a range of bottom roughness sizes when interpreting the data from this site.

The second deployment site in a wave/current environment was on Sable Island Bank (43°44′N, 60°49′W) in a depth of 45 m, during a cruise in September 1984. This site was chosen because an extensive sidescan-sonar survey of Sable Island Bank by Dr. Carl Amos of the Bedford Institute of Oceanography (personal communication) showed a sandy seabed of relatively low relief, with only small-scale ripple features likely. On this occasion EM sensors were deployed at three heights, 66, 44 and 21 cm above the bed but unfortunately the data quality on some channels was poor, with some unexplained oscillatory noise. No satisfactory vertical turbulence spectra could be obtained from the uppermost level, and only one vertical component at each of the other levels provided good data. Nevertheless, this is sufficient to allow estimates of stress to be made at the two lower levels in this important location.

The TUPS stereo camera system was also deployed three times in the vicinity of the Sable Island Bank site and provided some excellent stereophotography of the seabed. Figure 4a shows a portion of a typical photomosaic and Fig. 4b shows a transect through part of the mosaic, chosen to show the contrast between an apparently smooth region and a region of ripples. The ripples are clearly seen over most of the transect, but it is also seen that the "smooth" region near point A is about 4 cm below the level of the rippled region, suggesting the presence of features with longer length scales. It is not yet clear how to incorporate this kind of detailed topographic information into bottom stress prediction. However, a single stereophotograph of this region of the seabed would likely miss the longer length-scale features revealed in Fig. 4 and hence would tend to underestimate the bottom roughness.

4. Sensor alignment

Alignment problems with the EM sensors fall into two categories: nonorthogonality of the velocity components being measured and errors in the alignment

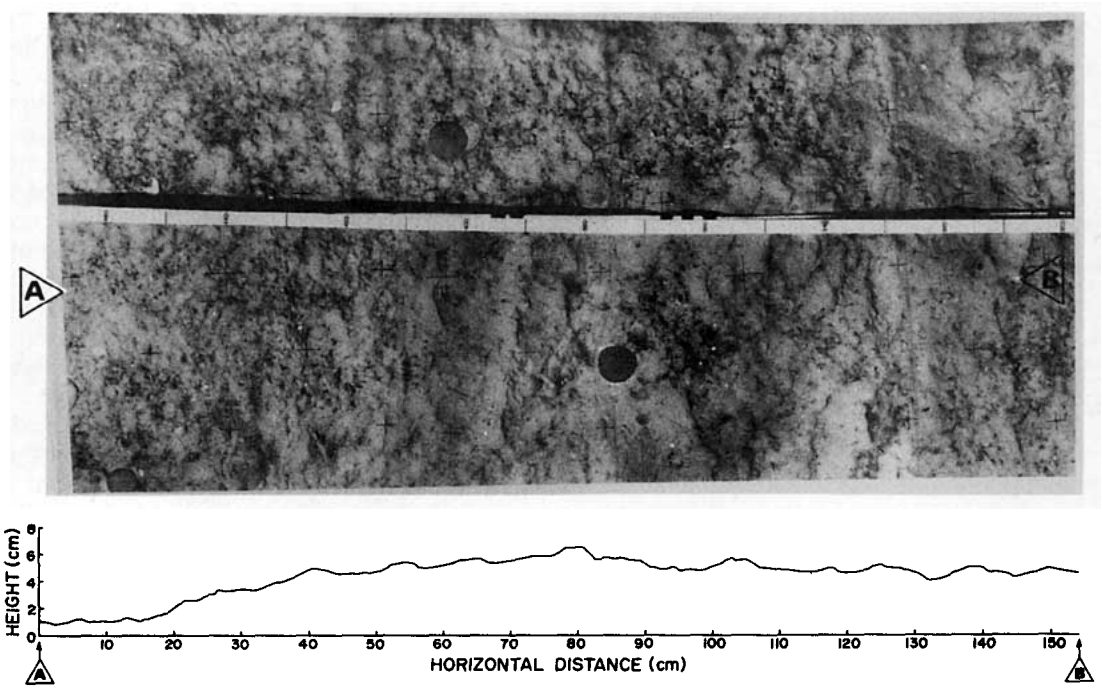

FIG. 4. (a) A portion of one of a stereo pair of photo-mosaics of the seabed at the Sable Island Bank site, taken with the TUPS systems. The central tape marks horizontal distance, in centimeters, from one end of the camera track. (b) A profile of bottom topography taken along the line marked A-B in (a). A region of low ripples is seen over most of the transect with a lower less undular seabed near A.

of sensor axes with the horizontal and vertical directions.

The orthogonality of the two component axes in a single EM sensor has been tested in a laboratory tank. Orthogonality of better than 0.2° (the limit of resolution of the technique used) was found. The two horizontal axes at each level, one from each sensor, could be made orthogonal to within ±0.50° during sensor mounting. Alignment of the two nominally vertical components with each other was much more difficult, and probably was no better than ±2° in practice. An attempt has been made with the Cow Bay data, for the sensor pair at 52 cm, to improve this alignment at the data analysis stage. Each sensor time series in the pair was rotated about its own axis independently to minimize the variance in the *difference* between the two vertical velocity time series at this level, and simultaneously to minimize the correlations between this difference time series and the horizontal velocity components. Rotations of about 1° were sufficient to achieve this minimization. In fact, as will be seen later, these small rotations of the apparent vertical axes are found to have a negligible effect on the stresses estimated by the inertial dissipation technique.

Estimation of the bottom stress by the inertial dissipation method is also relatively insensitive to rotations of the orthogonal axis system. Hence, although methods of alignment to true vertical and horizontal directions are being investigated in connection with Reynolds stress estimates, they will not be discussed here.

5. Mean flows

A major problem with the EM sensors is determining the voltage output corresponding to zero flow. Electrical interference can cause a significantly different zero-flow voltage in the laboratory from that experienced with the sensors deployed in the ocean. Our experience shows that this can lead to uncertainties in the mean flow of 2–3 cm s^{-1} or more, unless measurements of zero-flow voltage are made in situ (see also Cunningham et al., 1979). A variety of techniques can be used to obtain in situ values of zero-flow voltage. Commonly a conventional current meter, such as a rotor and vane, is used to provide an independent measure of mean flow (for example, see Elliott, 1984), but such meters do not generally give accurate results in a wave environment. Other methods of determining zero-flow voltage therefore had to be used.

At the Sable Island Bank site, a separate deployment was made with a plastic tube, about 80 cm in diameter, mounted inside the legs of the tripod so as to surround the EM sensors completely. Table 1 shows the apparent mean flows measured with and without the plastic tube, and the estimated true mean flows based on the differences between them. It is encouraging that the estimated true mean flows for the vertical components

TABLE 1. Mean flows and zero-offset flows at Sable Island Bank, September 1984.

Vertical component	Height (cm)	Zero-offset flow (cm s^{-1})	Measured mean flow (cm s^{-1})	Corrected mean flow (cm s^{-1})
Vertical 2	44	−1.76	−0.93	+0.83
Horizontal 2	44	−2.72	+1.26	+3.98
Vertical 1	44	+2.07	+1.79	−0.28
Horizontal 1	44	+1.07	−10.01	−11.08
Vertical 2	21	−1.52	−2.43	−0.91
Horizontal 2	21	−2.42	+0.81	+3.23
Vertical 1	21	−0.15	−0.22	−0.07
Horizontal 1	21	−0.97	−9.45	−8.48

NB: No zero-offset flow measurements were made for the sensors at 66 cm.

are all less than 1 cm s^{-1}, and the less noisy (vertical 1) channels show mean flows which are much smaller. These values, from sensors whose true mean flows should be zero, provide an indication of the accuracy with which all mean flows are being estimated for this dataset.

For the Cow Bay data, a rather different technique has been used. Figure 5 shows an example of concurrent time series obtained from the EM sensors at 0.52 m height and from a heated thermistor at 0.65 m height. The heated thermistor measures the magnitude of the velocity only and therefore rectifies a reversing flow. Furthermore, the signal from the thermistor is a highly nonlinear function of flow speed; it becomes very sensitive to changes of flow at low flow speeds. The rapidly varying signals and rectification of the oscillatory wave currents can be clearly seen in the first few minutes of the thermistor record in Fig. 5. In principle, a direct comparison between the heated thermistor record and the EM flowmeter records could provide an estimate of the zero-flow offset of the EM records. However, the calibration of the heated thermistor is only approximate, particularly at high flow speeds. More accurate calibration would be difficult for this environment, where flow direction is constantly changing. Furthermore, the heated thermistor was mounted about 2 m horizontally away from the EM sensors, and while this distance is small compared to the expected length scales of the mean flow and waves, it will cause differences between the instantaneous EM and thermistor records due to small-scale turbulence. We have, therefore, used the following procedure to estimate the zero-flow offset for the EM velocities.

We first choose a current threshold for the heated thermistor signal, and then find the average apparent velocity for each component of the EM sensors for those times when the heated thermistor signal indicates a speed smaller than the threshold. The choice of current threshold is somewhat arbitrary. In principle, we would want to choose the smallest threshold flow speed, but high frequency differences between the EM channels and the thermistor makes it unwise to choose a threshold so low that only a few EM estimates lie below the threshold. Table 2 shows the apparent horizontal currents for two thresholds, corresponding to speeds of approximately 1.4 and 0.9 cm s^{-1}. These threshold speeds are rather large but a scatter plot of the apparent horizontal velocity vector measured by the EM sensors shows that the flow speed minima are approached from all current directions, and hence an average over the approximately 10 minute records should provide a good estimate of the true zero flow.

This thermistor indication of near zero flow has been used not only for the EM sensors at 52 cm height, only 13 cm below the thermistors, but also for the EM sensors at 22 cm. Since the mean flow is expected to decrease towards the seabed while the wave orbital velocity above the wave boundary layer should remain

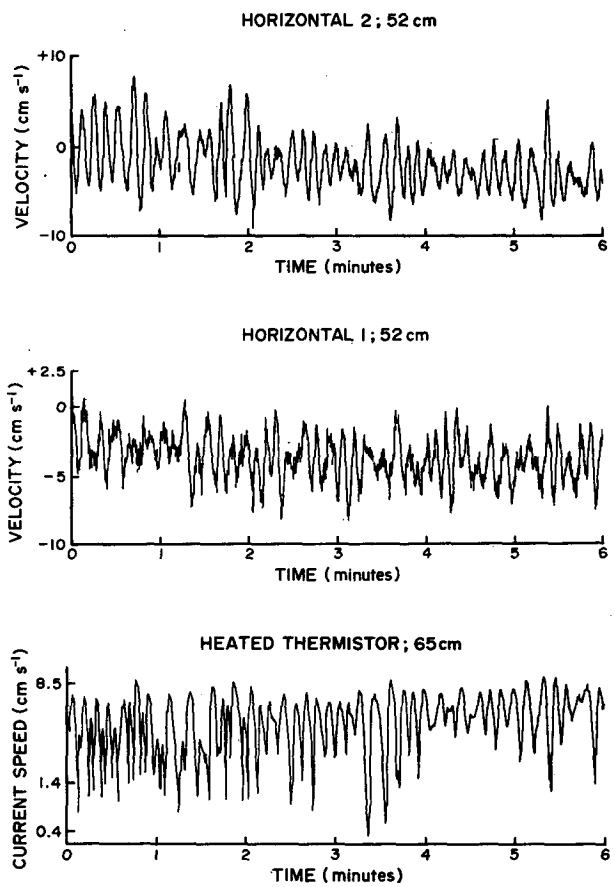

FIG. 5. Simultaneous velocity time series of the two orthogonal horizontal components from the electromagnetic sensors at 52 cm height, and a current speed time series from a heated thermistor sensor at 65 cm height, from the Cow Bay dataset. The two EM records show the apparent velocities, uncorrected for a zero-flow offset. Note the different vertical scales for the two EM sensors and the nonlinear (and approximate) vertical scale for the heated thermistor. The sharp negative spikes and rectification of the velocity by the heated thermistor are used to estimate a true zero velocity for the electromagnetic sensors.

TABLE 2. Mean flows and zero-offset flows at Cow Bay, N.S., July 1984.

Velocity component	Height (cm)	Zero-offset flow* (cm s^{-1})	Measured mean flow (cm s^{-1})	Corrected mean flow (cm s^{-1})
Horizontal 1	52	−3.19 (−2.88)	−4.14	−0.95 ± 0.30
Horizontal 2	52	+1.75 (+1.75)	−3.09	−4.84 ± 0.18
Horizontal 1	22	−2.75 (−2.57)	−3.45	−0.70 ± 0.30
Horizontal 2	22	+1.44 (+1.62)	−3.03	−4.47 ± 0.18

* The upper value is an average over 355 points. The lower (bracketed) value is for a more negative threshold, resulting in only 20 points. The upper value is used to obtain the "corrected mean flow."

constant with height, we might expect the times of zero mean flow to vary with height. This is likely to make the zero-flow estimates based on the thermistors less accurate for the lower EM sensors.

Table 2 also shows the measured and estimated true mean flows for a 10.5 minute segment of the Cow Bay data. The corrections to the mean flow are seen to be particularly significant in this low flow environment. The error bounds on the mean flow given in Table 2 are standard errors of the mean, based on the number of degrees of freedom for the correlated time series (Bayley and Hammersley, 1946). The error bounds on the apparent zero flow are also included.

The mean flow components given in Tables 1 and 2 show that the mean flows were coming from +(35 ± 1)° (Cow Bay) and −(65 ± 1)° (Sable Island Bank) relative to the direction from the center of the tripod towards the thermistor frame: the positive angle implies rotation in the clockwise direction, looking from above. Since the tripod legs are at 0° and ±120°, these mean flow angles and the wave angles given in Table 3 should ensure essentially uninterrupted flow towards the sensors.

6. Theory of bottom stress estimation

a. The modified dissipation method

Huntley (1988) reviews the methods which are available for estimating bottom stress from near bottom measurements of velocity. With measurements at only two heights above the seabed, and with the uncertainties in mean flows indicated by the error bounds in Tables 1 and 2, the present dataset does not allow estimation of bottom stress from the mean velocity profile.

Huntley (1988) points out that, of the alternative methods for estimating bottom stress, the "eddy correlation" method suffers from the disadvantage that it is very sensitive to errors in the orientation of the vertical axis, particularly in an environment where oscillatory wave flows are significant.

The modified inertial dissipation method, discussed by Huntley (1988), appears to be the most appropriate method for estimating bottom stress from our data. The method involves use of a one-dimensional wavenumber (k) spectrum of the ith turbulent velocity component, $\phi_{ii}(k)$. In the inertial subrange of wavenumbers this spectrum is expected to fall off as $k^{-5/3}$ and, if measurements are made within the constant stress layer, the spectrum in this subrange can be related to the friction velocity u_* by

$$u_* = [\phi_{ii}(k)k^{5/3}/\alpha_i]^{1/2}(\kappa z)^{1/3} \quad (1)$$

where κ is the von Kármán constant, α_i is the appropriate Kolmogorov constant and z is the height above the bed. For one-dimensional spectra of the longitudinal (parallel to the mean flow) turbulent velocity component Champagne et al. (1977) and Williams and Paulson (1977) find values of Kolmogorov constant of 0.50 ± 0.02 and 0.54 ± 0.01 respectively.

Following GWG we have calculated u_* from the spectra of vertical fluctuations rather than the spectra of longitudinal fluctuations, since the latter are much more likely to contain significant contributions from wave motion which would cause overestimation of u_*. In the inertial subrange the one-dimensional spectrum of velocity fluctuations transverse to the mean flow is expected to be larger than the spectrum of along-flow fluctuations by a factor of $^4/_3$ (e.g., Tennekes and Lumley 1972, p. 254). Bowden and Ferguson (1980) present field measurements of this factor from tidal flows. The ratio of vertical to along-flow spectra was found to be a constant if $\kappa z \geq 2\pi$, with an average value of 1.44 but with error bounds that readily encompass the theoretical value of 1.33. Thus, as long as we apply Eq. (1) only for $\kappa z \geq 2\pi$, calculation of u_* using spectra of *vertical* velocity fluctuations will use a Kolmogorov constant which is taken to be $^4/_3$ of the one-dimensional longitudinal constant. For the present work we have chosen

$$\alpha_3 = \left(\frac{4}{3}\right) \times 0.52 = 0.69$$

where the one-dimensional longitudinal constant, 0.52, is the mean of the values found by Champagne et al. (1977) and Williams and Paulson (1977).

However, Eq. (1) is not valid unless measurements are made both within the constant stress layer and also above a critical Reynolds number ($\mathrm{Re}_c = u_* \kappa z_{cr}/\nu$, where ν is the kinematic viscosity of water and z_{cr} the corresponding critical height above the bed) to ensure separation between low wavenumber turbulence production and high wavenumber dissipation. Huntley (1988), taking Re_c to be 3000, shows that these two conditions are unlikely to be satisfied simultaneously in low energy environments. In particular, the Reynolds numbers for the present dataset (and for the dataset

described by GWG) are too low to ensure the existence of an inertial subrange.

Huntley (1988) proposes a modification of the inertial dissipation method to be used at low Reynolds numbers. His modification involves using Eq. (1) to obtain a first estimate of friction velocity, $\hat{u}_*$, and then using this to obtain the true friction velocity u_* from:

$$u_* = [\hat{u}_*^3 \mathrm{Re}_c \nu/(\kappa z)]^{1/4} \quad \text{for} \quad z < \mathrm{Re}_c \nu/(\kappa u_*). \quad (2)$$

Huntley shows that application of Eq. (2) to the friction velocity estimates of GWG removes a trend towards increasing friction velocity with height, and results in estimates which decrease slowly with height, in good agreement with theoretical predictions.

b. *Practical aspects of the application of the method*

Our measurements are in the form of time series of turbulent velocities and therefore provide spectra as functions of frequency rather than wavenumber. To convert to wavenumber spectra, we need to invoke the Taylor concept of "frozen turbulence," in which

$$\phi(k) = \phi(f)/(2\pi/\bar{u}) \quad (3)$$

where $\bar{u}$ is the mean velocity and f is the frequency in hertz.

In order for the frozen turbulence concept to be valid we require the time scale of an eddy to be much larger than the time for that eddy to be advected past the measurement point by the mean flow. Tennekes and Lumley (1972) estimate the time scale of an eddy with wavenumber k to be $2\pi/(k^3E(k))^{1/2}$, while the time for such an eddy to pass a point is $2\pi/k\bar{u}$. Hence for frozen turbulence we require $kE/\bar{u}^2 \ll 1$. For the data discussed here, this parameter is typically smaller than 10^{-3} in the inertial subrange.

It might also be anticipated that the Taylor hypothesis would need to be substantially revised in an environment with significant oscillatory wave flows. However, Lumley and Terray (1983) show that, for isotropic turbulence and horizontal wave velocities much larger than vertical velocities, the friction velocity corrected for the influence of wave advection is given approximately by

$$u_* = [1 - 0.16(u_{\mathrm{rms}}/\bar{u})]^{1/2}\hat{u}_*. \quad (4)$$

where u_{rms} is the root-mean-square horizontal wave velocity and $\hat{u}_*$ is the value of friction velocity found from vertical spectra using the Taylor hypothesis. Table 3 shows the correction factors which have been made to the friction velocities in Table 5. The largest reduction in u_* is about 5% so this effect is not of major importance compared to other sources of error (Table 6).

If the Reynolds number is too low for an inertial subrange to develop, it is not immediately clear what range of wavenumbers should be used in Eq. (1). Nevertheless, even at low Reynolds numbers a region of the spectrum of approximately $k^{-5/3}$ roll-off is found and it is not difficult in practice to use Eq. (1) to obtain an estimate of $\hat{u}_*$. Indeed GWG applied Eq. (1) to their data without modification, finding spectra (e.g., their Fig. 7) with reasonable $k^{-5/3}$ slopes despite low Reynolds numbers.

There are, however, some clear constraints on the wavenumber range for which a $k^{-5/3}$ roll-off might be expected. For a sensor a distance z above the bed the peak of turbulent energy is expected to occur near $k = \pi/z$ (e.g., Soulsby, 1983; Gross and Nowell, 1985), and our earlier discussion of the results of Bowden and Ferguson (1980) suggests that we must use wavenumbers greater than twice this expected peak wavenumber if the assumed value of Kolmogorov constant ($\alpha_3 = 0.69$) is to be valid. The possible presence of surface wave energy prevents unambiguous confirmation of turbulence peaks at these wavenumbers in the present datasets (see also the discussion by Grant and Madsen, 1986). The lower wavenumber limit of the $k^{-5/3}$ subrange was therefore chosen to be at or larger than either twice the wavenumber of the expected turbulence peak ($k = 2\pi/z$) or the highest significant incident wave wavenumber seen in the horizontal flow spectra (Table 4). The upper wavenumber limit for the subrange is set by the averaging volume or the response time of the EM sensors. Soulsby (1980) estimates that his EM sensors (Colnbrook discus-shaped sensors) with electrodes separated by a distance D will attenuate the turbulence spectra by 50% for $k = 2.3/D$. Our EM sensors (spherical) have an electrode spacing of about 4 cm, giving an upper wavenumber limit of 0.58 cm^{-1}. In fact, from discussions with the manufacturer of our EM sensors, it appears that spectral attenuation at this

TABLE 3. Wave and current conditions, and correction factors for friction velocity to account for the kinematic influence of wave velocities (Equation 4).

	Height (cm)	Wave flows u_{rms} (cm s^{-1})	Mean flow $\bar{u}$ (cm s^{-1})	$u_{\mathrm{rms}}/\bar{u}$	Correction for u_* [Eq. (4)]	Wave period (s)	Angle between mean and wave flows (deg)
Cow Bay	52	3.30	4.9	0.67	0.963	11.5	9°
	22	3.55	4.5	0.79	0.949		
Sable Island Bank	44	2.01	11.8	0.17	0.998	10.0	27.5°
	21	1.99	9.1	0.22	0.996		

TABLE 4. Wavenumber limits for the inertial subrange.

	Height z (cm)	Lower limit on wavenumber $(2\pi/z)$ (cm^{-1})	Surface waves maximum wavenumber (cm^{-1})	Sensor averaging (cm^{-1})	Sensor frequency response (cm^{-1})	k range used (cm^{-1})
Cow Bay	55	0.12	0.14	0.58	0.72	0.22–0.34
	22	0.29	0.16	0.58	0.78	0.29–0.34
Sable Island Bank	44	0.14	0.19	0.58	0.30	0.19–0.24
	22	0.30	0.24	0.58	0.39	0.30–0.32

wavenumber may be an order of magnitude less than estimated by the Soulsby method, though no definitive tests have been conducted. The frequency response of the EM sensors is determined by their 5 Hz output filters, with 50% spectral attenuation at 0.56 Hz. The corresponding wavenumbers are shown in Table 4, along with the upper limit due to sensor spatial averaging. In order to limit the uncertainty introduced by correcting the spectra for spatial and temporal filtering the upper wavenumber limits used in the determination of u_* were chosen to be much smaller than the upper limits for 50% spectral attenuation. The wavenumber ranges used are also shown in Table 4. With these ranges, the largest correction to u_* due to sensor frequency response was approximately 10%.

7. Dissipation estimates of the friction velocity

Spectra of vertical velocity fluctuations have been calculated for 3072 point time series, corresponding to 15.57 and 9.73 min for the Cow Bay and Sable Island Bank datasets, respectively. This choice of record length was based on visual assessment of the length of time for which the mean flows remained approximately steady. Grant et al. also found, by careful consideration of the variance of their stress estimates, an optimum averaging time of about ten minutes.

Spectra were calculated using the IEEE analysis programs (Carter and Ferrie, 1979). Each time series of 3072 points was separated into five time series of 1024 points, overlapping by 50%. A cosine bell window was applied to each shorter time series before Fourier transforming. The five resulting spectra were averaged. A final averaging over three adjacent frequencies resulted in spectral estimates with 25 degrees of freedom and frequency resolutions of 9.6×10^{-3} Hz (Cow Bay) and 1.5×10^{-2} Hz (Sable Island Bank). Examples of spectra of vertical velocity, converted to wavenumber spectra using the frozen turbulence hypothesis, are shown in Figs. 6 and 7, along with estimates of the 95% confidence intervals and an indication of a $-5/3$ slope.

Figure 8 shows Cow Bay spectra plotted in the form $k\phi(k)$ vs. k. It can be seen that spectra from the two different heights agree well, confirming that the appropriate spectral scaling is with k, not kz, as expected for a true inertial subrange. This is in agreement with the observations of Gross and Nowell (1985) for spectra from below the critical height, and indicates that a true inertial subrange is not present in these spectra and hence that Eq. (2) must be used to correct the dissipation estimates (Huntley, 1988).

Before using these in situ spectra to determine friction velocities, we consider it important to assess the contributions of sensor noise to the spectra, particularly in view of the relatively quiet conditions at both Cow Bay and Sable Island Bank. Noise levels have been assessed using spectra measured by the sensors when held in still water. For Cow Bay, noise spectra were measured in the laboratory at completion of the cruise. Figure 9a shows a typical comparison between an in situ spectrum and noise spectrum. The spectra have been smoothed with approximately logarithmic smoothing, and plotted on a linear/log scale to show their proportional magnitudes. Over the range of frequencies used to estimate u_*, the average ratios of in situ spectral levels to noise spectral levels for Cow Bay ranges from 4.7, for the sensor at 22 cm above the bed, to 4.9 and 6.6, respectively, for the two sensors 52 cm above the bed. Removing these background noise levels from the in situ spectra results in reductions in $\hat{u}_*$ and u_* [Eqs. (1) and (2)] of 11% and 8.5%, respectively, at 22 cm and 10.4% ($\hat{u}_*$), 8% (u_*) and 8% ($\hat{u}_*$), 6% (u_*) for the two sensors at 52 cm. Although there is some uncertainty about how representative the laboratory noise spectra were of noise levels in situ (one might expect rather lower levels in situ) we have chosen to make these corrections to the friction velocity estimates discussed here. For Sable Island Bank the noise spectra used are those measured during the dummy in situ deployment with the sensors shrouded by the plastic tube (see section 5). Figure 9b shows a comparison between the vertical velocity spectrum measured at 44 cm above the seabed and the corresponding noise spectrum. Linear spectral smoothing has been used for these spectra. The noise level in this case is significantly higher than found for the Cow Bay runs (a system fault contributing to this noise level was subsequently discovered). The high spectral level below about 0.15 Hz may also indicate that the plastic tube did not eliminate completely long period flows around the sensor; sub-

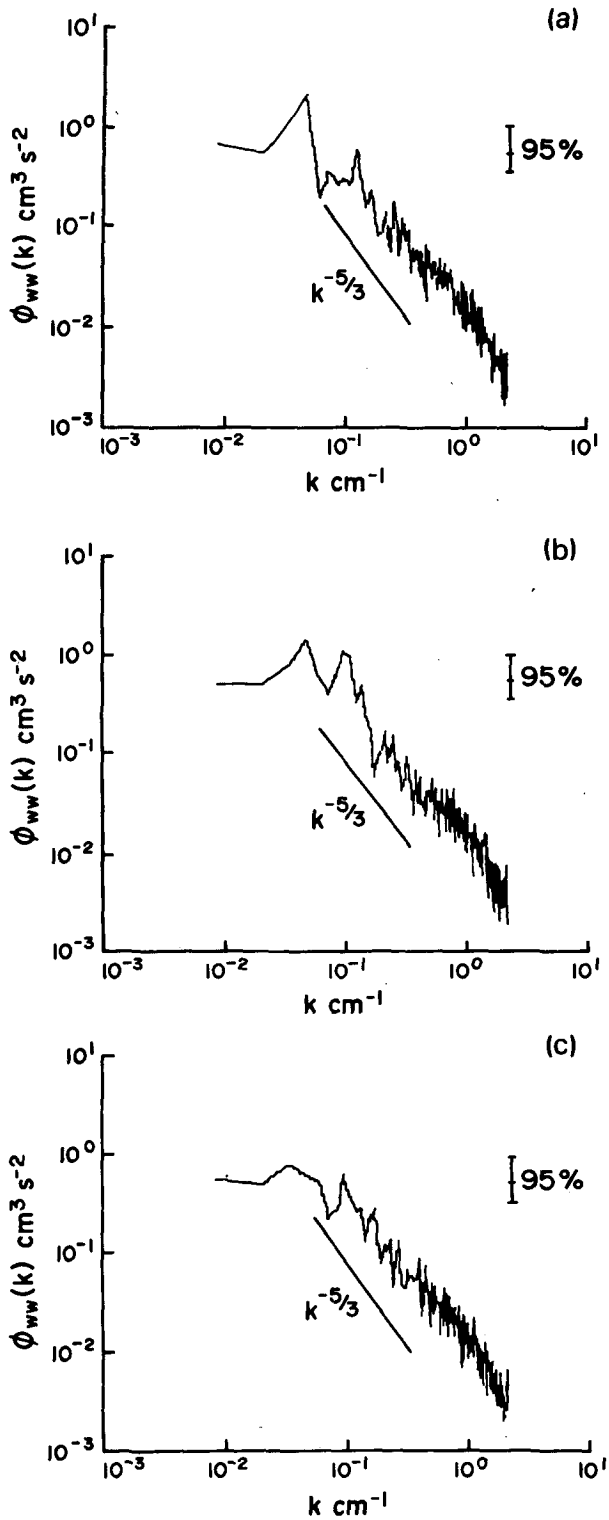

FIG. 6. Wavenumber spectra of vertical velocities, Cow Bay: (a) sensor 1 at 52 cm, (b) sensor 2 at 52 cm and (c) sensor at 22 cm.

sequent laboratory noise tests gave spectra without high energy below 0.15 Hz but with spectral levels very similar to the dummy deployment at higher frequencies.

Ratios of in situ spectral levels to noise spectral levels, over the frequency ranges used to estimate friction velocities, were 2.8 from 44 cm above the bed and 2.5 from 22 cm above the bed. The corresponding reduction in $\hat{u}_*$ and u_* resulting from removing these noise levels from the in situ spectra are 20% ($\hat{u}_*$), 15% (u_*) at 44 cm and 22% ($\hat{u}_*$), 17% (u_*) at 22 cm. These corrections have also been made to the friction velocities discussed in the following paragraphs.

Table 5 shows the measured dissipation estimates of $\hat{u}_*$ based on the vertical velocity spectra. The table also shows the values "corrected" using Eq. (2). Based on these corrected values, the critical height is also given, and in each case the measurement height is below the critical height, indicating that the correction is appropriate. Table 5 also shows an estimate of the height of the top of the constant stress layer, ($=0.015u_*/f$; Huntley, 1988). The measurements in each case are well within the expected constant stress layer.

The values for $\hat{u}_*$ and u_* in Table 5 have been cor-

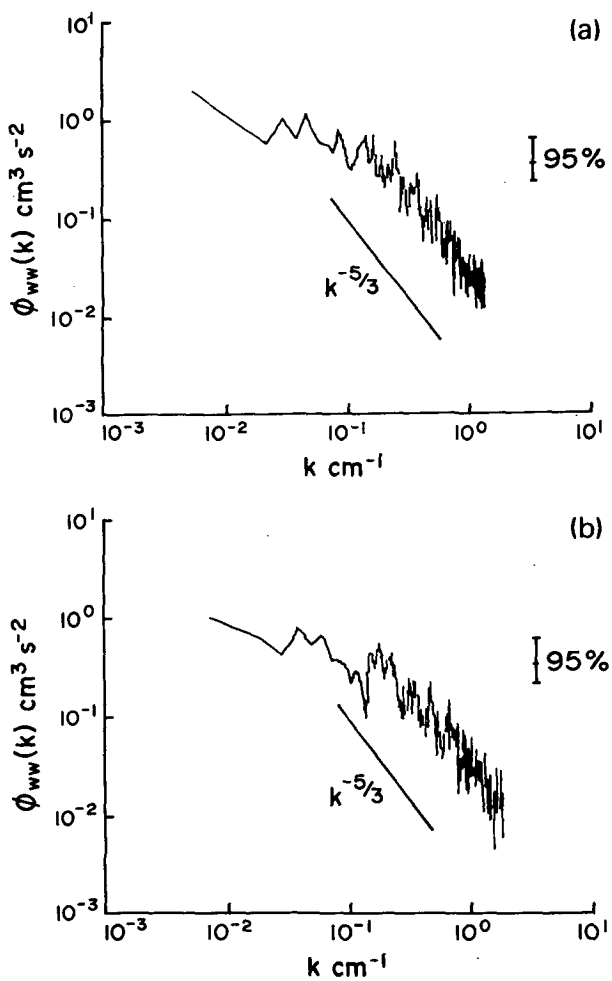

FIG. 7. Wavenumber spectra of vertical velocities, Sable Island Bank: (a) sensor at 44 cm and (b) sensor at 21 cm.

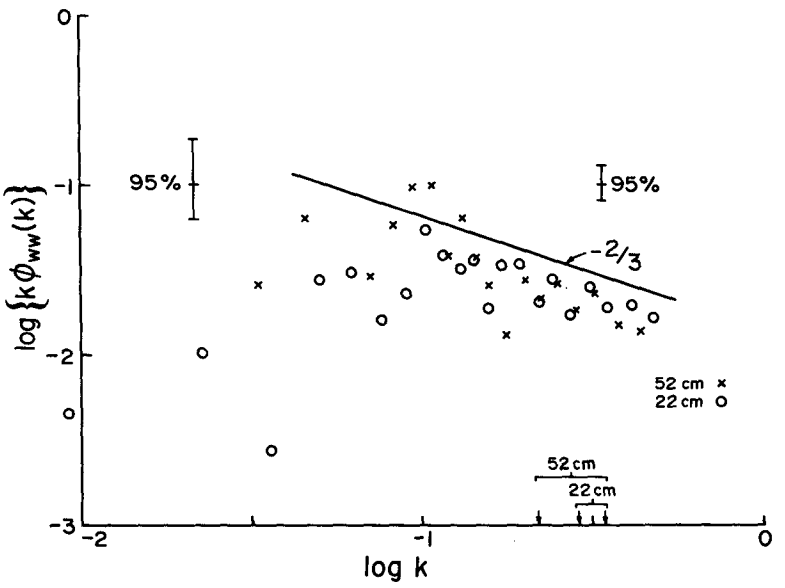

FIG. 8. Cow Bay vertical spectra $k\phi(k)$ vs k (where $\phi(k)$ is the wavenumber spectrum). The spectra are truncated at $k = 0.5$ cm^{-1} because higher k values are well above the wavenumber ranges used to estimate u_*: ×: spectrum of sensor 2 at 52 cm; O: spectrum of the sensor at 22 cm. The large wavenumber similarity of the spectra from the two heights can be seen.

rected for the influence of the sensor output filters (less than 10%) and for the correction factors shown in Table 3. Remaining possible sources of error are given in Table 6. As expected, the total error bounds are dominated by the uncertainty of the spectral level. No correction has been made to the u_* values in Table 5 to account for spatial averaging of the EM sensors, since, as mentioned earlier, the magnitude of appropriate corrections is very uncertain. The possible error due to spatial averaging given in Table 6 is based on Soulsby (1980) but is probably overestimated perhaps by as much as an order of magnitude. Also shown is an estimate of the possible error introduced by the assumption, used in deriving Eq. (1), that turbulence production is locally equal to dissipation. Wyngaard and Cote (1971) find that production is less than dissipation by a maximum of 30% in neutral and stable atmospheric boundary layers, though they point out that much of this difference might be accounted for by experimental error. We have used the 30% value for the estimate in Table 6, which should therefore also be considered an upper limit. Errors in sensor height above the bed do not affect u_* values estimated using Eq. (2), except possibly by making small changes to the wavenumber limits in Table 4.

The spread of $\hat{u}_*$ values shown in Table 5 is probably within the wide error bounds possible based on Table 6. However, at both sites $\hat{u}_*$ values are higher at greater distances from the boundary, as was also observed by GWG. Although the corrections using Eq. (2) are large, it is encouraging that they significantly reduce the difference in the u_* values from each level, making them much more consistent with the expectation of a constant stress.

8. Comparison of measured stresses with predictions

In the absence of wave effects the velocity in the lower part of the boundary layer, is expected to follow a logarithmic profile:

$$\bar{u} = u_*/\kappa \ln(z/z_b) \tag{5}$$

with u_* determined by the mean flow alone and with z_b given by the true bottom roughness length.

At the Cow Bay site the nature of the appropriate bottom roughness is uncertain owing to the variability of bottom material. However, we can obtain an estimate of the upper limit for the roughness length if we assume that the bottom is covered by cobbles of the size (typically 5–15 cm diameter) shown in the single stereophotograph taken from the tripod. For the calculation to follow, we take a bottom sediment diameter of 15 cm, leading to a bottom roughness length of about 0.5 cm, using the Nikuradse estimate [bottom roughness length = $\frac{1}{30}$ × sediment diameter (e.g., Hinze, 1975)]. With this value and the mean velocities measured at each height, the friction velocities predicted using Eq. (5) (i.e., assuming no wave effects) are 0.42 cm s^{-1} at 52 cm, and 0.475 cm s^{-1} at 22 cm. These values are much smaller than the measured friction velocities of 0.64 and 0.59 cm s^{-1} (at 52 cm) and 0.58 cm s^{-1} (at 22 cm) (Table 5) despite the use of an upper limit on the bottom roughness. In fact, the bottom roughness lengths needed to match the observed mean

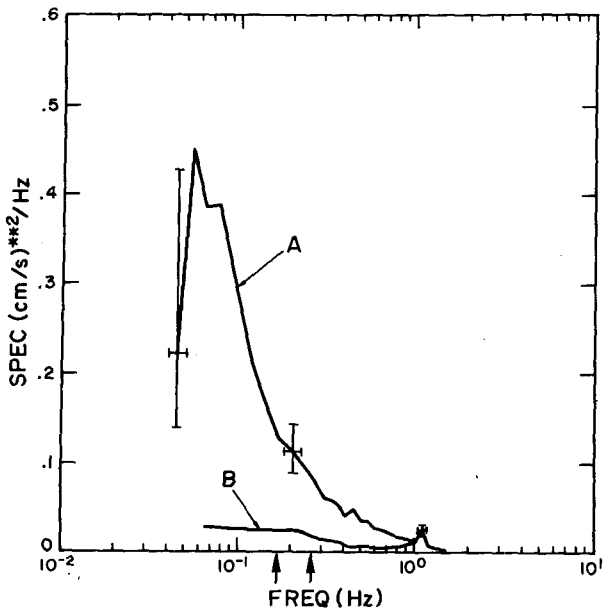

FIG. 9a. Vertical velocity spectrum from 52 cm above the bed at Cow Bay (A) and the corresponding still water "noise" spectrum (B). Spectra have been smoothed to give approximately constant bandwidth on the logarithmic frequency scale, and representative bandwidths and 95% confidence bands are shown. Vertical arrows mark the frequency range used in the calculation of u_*.

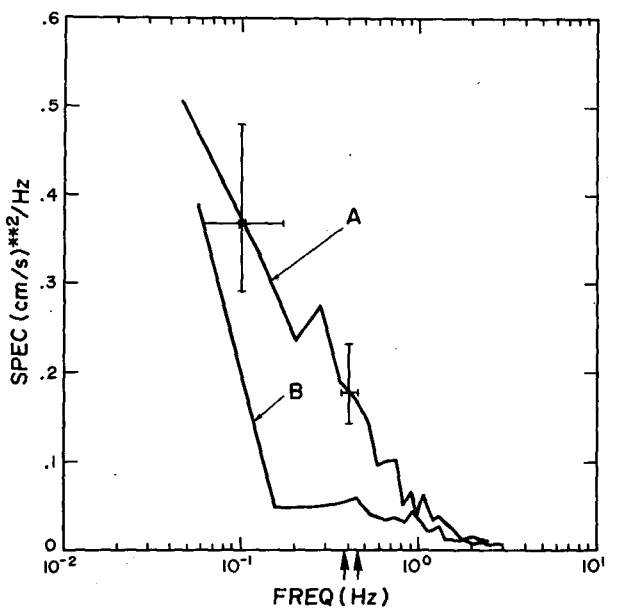

FIG. 9b. Vertical velocity spectrum from 44 cm above the bed on Sable Island Bank (A) and the corresponding "noise" spectrum from the dummy deployment (B). Representative bandwidths and 95% confidence levels are indicated. Vertical arrows as in (a).

flows and friction velocities are 2.4 and 1.9 cm for the sensors at 52 cm, and 1.0 cm for the sensor at 22 cm. When multiplied by 30 to give estimates of the corresponding sediment diameters, these values clearly lead to improbably large estimates. Bedforms and distributed seafloor mounds can result in considerably higher values of bottom roughness length than those based on sediment diameter (e.g., Wooding et al., 1973; Grant and Madsen, 1982). However, there is no evidence from our observations or from earlier surveys in the Cow Bay region to suggest the presence of the large bedform features needed to produce bottom roughness lengths as large as 1.0–2.4 cm.

A similar situation arises with the results from Sable Island Bank. Figure 4b shows sand ripples of less than 1 cm height 10–15 cm apart over most of the transect. Grant and Madsen (1982) find that the bottom roughness length for ripples of this kind is given approximately by h^2L^{-1}, where h is the ripple height and L is the ripple spacing. The corresponding roughness length for the ripples in Fig. 4 is therefore in the range 0.07–0.1 cm. With use of the larger value and the measured mean velocities at each height, the predicted friction velocities at 44 and 21 cm are 0.78 and 0.67 cm s^{-1} respectively. Again these are considerably smaller than the observed values of 0.83 and 0.89 cm s^{-1}. To obtain the observed currents and friction velocities in the absence of waves, we would require roughness lengths of 0.15 and 0.35 cm respectively, values which would be difficult to justify on the basis of the bottom roughness information in Fig. 4.

Thus, although we cannot entirely rule out the possibility that unexpectedly large physical bottom roughness lengths occur, these calculations indicate that the measured friction velocities both at Cow Bay and at Sable Island Bank are inconsistent with predicted friction velocities for a simple mean flow boundary layer. It appears that wave influences are indeed important.

Of several recent theories for boundary layers in the presence of both waves and steady currents, the theory of GM appears to be gaining the widest acceptance. We have therefore chosen to compare our observations with predictions based on their theory. Grant and Madsen (GM) model the combined wave/current boundary layer as two logarithmic layers, a thin wave boundary layer with thickness scale ku_*/ω (ω is the

TABLE 5. Measured values of friction velocity.

	Height z (cm)	$\hat{u}_*$ (cm s^{-1})	u_* (cm s^{-1})	Estimated critical height (cm)	Estimated height of constant stress layer (cm)
Cow Bay	52	0.42	0.64	176	96
	52	0.38	0.59	191	89
	22	0.28	0.58	194	87
		51%	11%		
Sable Island Bank	44	0.58	0.83	136	124
	21	0.48	0.89	126	134
		19%	7%		

TABLE 6. Possible sources of error in the u_* estimate.

Source	Effect on u_* (%)
95% limits on spectra*	
Upper sensors	$-7 \rightarrow +9$
Lower sensors	$-13 \rightarrow +18$
Spatial averaging of sensors	$+4 \rightarrow +9$
Axis rotation. Error per degree	0.4
Mean flow	±2
Kolmogorov constant	±5
Critical Reynolds number for inertial subrange	±7
Imbalance between turbulence production and dissipation	±9

* Lower range for upper sensors due to averaging over wider wavenumber range.

wave radian frequency), and a thicker mean current boundary layer overlying it. In each boundary layer, turbulent closure is achieved by assuming an eddy viscosity which increases linearly with height above the bed, but the total friction velocity in the lower wave boundary layer is larger than that in the mean flow boundary layer because of the influence of the waves. Grant and Madsen (GM) show that matching the mean velocity profile across the interface between the two boundary layers results in values of both apparent bottom roughness and friction velocity in the upper boundary layer which are much larger than would occur in a mean flow boundary layer with the same mean velocity but without waves.

Grant and Madsen (GM) describe an iterative procedure for solving for friction velocities in both layers and apparent roughness length in the upper layer, based on measurements of wave and mean flows at a known height above the bed. For our calculations we have used an algorithm developed by Davidson (1984). Inputs to the iteration are the mean flow amplitude, the wave orbital velocity, the angle between the wave and mean currents, the height at which the measurements were made, the wave period and the physical bottom roughness (assumed to be 30 × the bottom roughness length scale z_b).

In a continental shelf environment the wave climate will, of course, be in the form of a directional wave spectrum and unique choices of wave amplitude, period and direction are not possible. For each run, we have taken the mean wave direction to be the direction of the major axis in a scatter plot of the instantaneous vectors of horizontal current over the approximately 10 minute averaging period. The resulting 180° ambiguity in wave direction is irrelevant in the GM theory. Figure 10 shows the scatter plot for the Cow Bay data at 52 cm above the bed. The angle between the mean wave direction and the mean flow vector is not well defined, but is approximately 9°. Fortunately, the calculated friction velocities are not sensitive to changes in the assumed angle between the wave and mean flows. For example, for the Sable Island Bank conditions, a change of wave/current angle from 27.5° to 65.5° resulted in a change of only 3% in predicted u_*. More

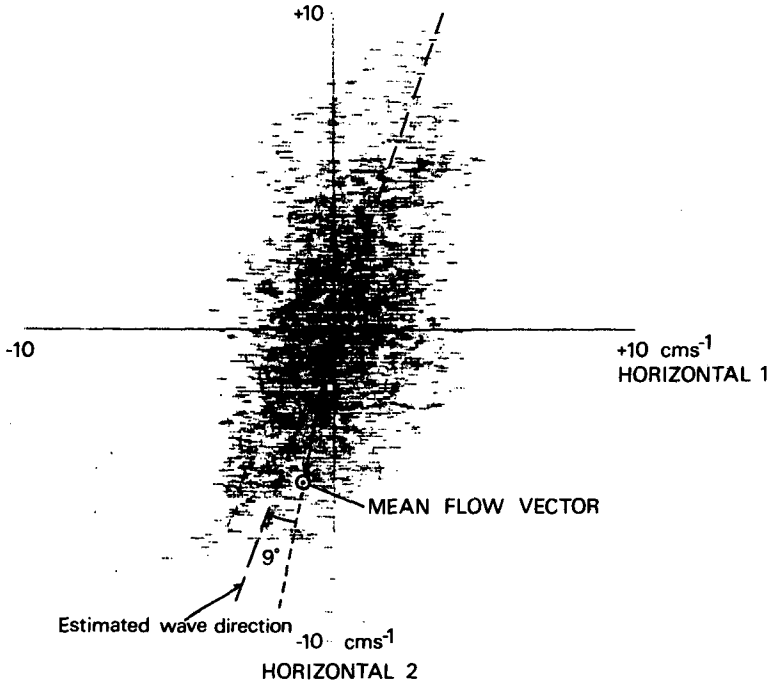

FIG. 10. Scatter plot of the horizontal velocity vector at Cow Bay, 52 cm. The mean flow velocity vector is also shown. The angle between the mean flow and the waves is estimated to be 9°.

important is the choice of a wave orbital velocity. Grant and Madsen argue that the bottom stress felt by the mean flow will be dominated by the largest stresses, developed during peak waves, since the average of the highly nonlinear bottom stress will be heavily weighted towards the high values. They choose as the appropriate wave velocity "the amplitude of the envelope of the wave record over the mean flow averaging period." In the computations described here we have used both the significant wave velocity, $u_{1/3}$, defined as two times the standard deviation of the horizontal velocity record, and also the average of the highest 10% of the waves, $u_{1/10} = 1.27u_{1/3}$. The wave period is taken as the period of the spectral peak in horizontal flow spectra.

We have argued that we expect the physical bottom roughness for the Cow Bay site to be in the range 5–15 cm for the pebbles (though perhaps less if the boundary layer is influenced by the sandy bottom known to be in the vicinity), and for Sable Island Bank to be approximately 2–3 cm (=30 × the roughness length estimates, 0.07–0.10 cm). However, although the Sable Island Bank value is rather better known than the Cow Bay value, the bottom roughness is not known with confidence at either site. We have therefore plotted in Figs. 11 and 12 the calculated values of u_*, for Cow Bay and Sable Island Bank respectively, as functions of the assumed physical bottom roughness. Also indicated is the sensitivity of the predictions to changes in the wave orbital velocity amplitude.

The friction velocities predicted from the measurements at the two levels at Cow Bay (Fig. 11) differ by around 25%. Although the uncertainties in the predictions encompass this difference, it is still considerably larger than that found for the Sable Island Bank data, where the difference ranges from 10% at $k_b = 2$ cm to 4% at $k_b = 10$ cm. Possible explanations for the large difference in predicted u_* values for the Cow Bay data include the small mean flows at that site, and the use of a common zero flow offset for each current meter, based on the heated thermistor measurements made at 65 cm above the bed. As pointed out earlier, we expect the mean flows to be rather better known at 52 cm than at 22 cm, and the predictions may therefore be more reliable for the upper level.

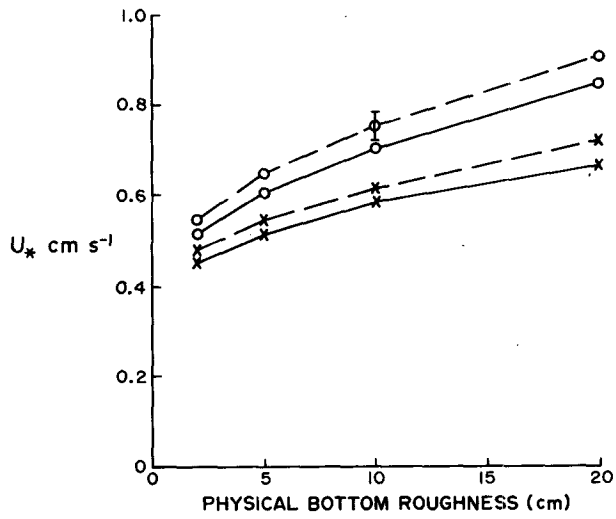

FIG. 11. Graph of friction velocity, predicted by the GM theory for the Cow Bay conditions, against assumed physical bottom roughness: × = predictions based on measurements at 52 cm; ⊙ = predictions based on measurements at 22 cm. Solid lines: predictions using the significant wave velocity, $u_{1/3}$; dashed lines: predictions using $u_{1/10}$. The error bounds on the predictions at bottom roughness 10 cm are those due to uncertainty in the mean flow alone.

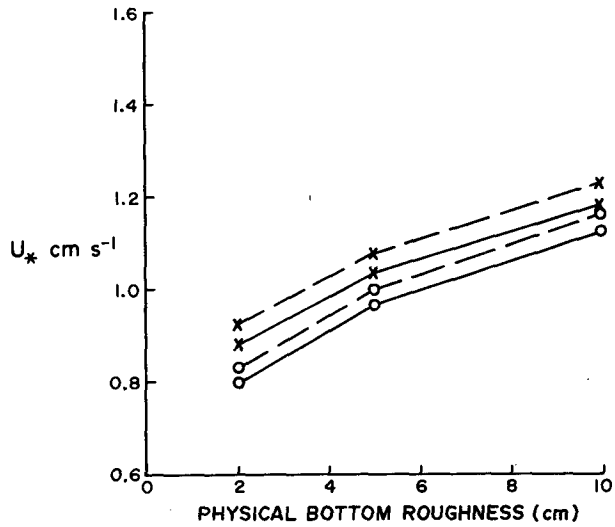

FIG. 12. Graph of predicted friction velocity for Sable Island Bank against assumed physical bottom roughness: ×: measurements at 44 cm; ⊙: measurements at 21 cm; solid lines: predictions using $u_{1/3}$; dashed lines: predictions using $u_{1/10}$.

If we compare these predictions with our measured values of friction velocity we find encouraging agreement when the significant wave velocity, $u_{1/3}$, is used in the predictions. Thus at Cow Bay, using a physical bottom roughness in the range 10 ± 5 cm, the predicted friction velocities are 0.575 ± 0.05 cm s^{-1} (at 52 cm) and 0.696 ± 0.08 cm s^{-1} (at 22 cm), compared with an average measured value of 0.60 cm s^{-1}. This agreement should be viewed in the context of a predicted u_* no larger than 67% of the observed, if wave influences were ignored. At Sable Island Bank, for an assumed physical bottom roughness in the range 2–3 cm the predicted friction velocities are 0.91 ± 0.03 and 0.83 ± 0.03 cm s^{-1} at the two levels compared with an average measured value of 0.86 cm s^{-1}. Of course such close agreement must be considered fortuitous in view of the expected uncertainty in the measured estimates, but the results suggest that the GM scheme provides a good estimate of bottom friction if the significant wave orbital velocity is used.

9. Summary and conclusions

This paper has discussed the estimation of mean flow friction velocity for two sites on the Nova Scotia continental shelf where both waves and mean flow were present. Friction velocities were estimated by the modified dissipation method described by Huntley (1988). The estimate from two heights above the seabed agree with each other to within a few percent at each site, as expected for measurements made within the constant stress layer.

The number of observations discussed in this paper is small, covering only a restricted range of wave/mean flow conditions. Nevertheless, the measured values of friction velocity are consistently larger than can be readily explained by a boundary layer in which mean flow effects alone are important. It is difficult, even with detailed quantitative information like that obtained at the Sable Island Bank site, to rule out entirely the possibility that the observations are the result of extremes of bottom roughness, but it is unlikely that this would be the case for both the sites. It is therefore reasonable to conclude that the enhanced bottom stresses are due to the presence of wave motion.

We have compared our measured estimates of friction velocity with predictions based on the theory of Grant and Madsen (1979). The predictions are found to be relatively insensitive to the assumed bottom roughness but more sensitive to the magnitude of wave velocity orbital velocity used. Predictions based on the significant wave orbital velocity, the average of the highest one-third of wave velocity amplitudes, are in close agreement with the observations.

Grant et al. also find agreement between the predictions of the GM model and their measured estimates of friction velocity based on the mean flow profile, though they apparently used an extreme value of orbital velocity in their predictions.

The agreements between measured bottom stresses and the predictions of the GM model are encouraging, and suggest that, at least for low energy conditions, the GM model accurately predicts the influence of the waves. Further field measurements are needed to test the model over a wider range of wave and mean flow conditions.

Acknowledgments. The contribution of Dr. Terry Chriss was vital to all aspects of the fieldwork described in this paper. We also particularly thank him for allowing us to use the stereophotographs from TUPS, an instrument he designed and deployed. Members of the Coastal Oceanography, Metrology and Institute Facilities Groups at the Bedford Institute of Oceanography were generous with their advice and time during this project. The help of the crew of CSS *Dawson* is also gratefully acknowledged. Data analysis and preparation of the first draft of this manuscript were completed while the author was on sabbatical leave at the Oceanography Department, University of Southampton, England, and at the Coastal Studies Unit of the Department of Geography, University of Sydney, Australia. The hospitality and assistance of the members of both of these Departments contributed materially to this work. The project was primarily funded by Strategic Grants from the Natural Sciences and Engineering Research Council of Canada, with additional support from the Department of Energy, Mines and Resources, and the Department of Supply and Services, Government of Canada.

REFERENCES

Bayley, G. V., and J. M. Hammersley, 1946. The effective number of independent observations in an autocorrelated time series. *J. Roy Statist. Soc.*, **B8**, 184–197.

Bowden, K. F., and S. R. Ferguson, 1980. Variation with height of the turbulence in a tidally-induced bottom boundary layer. *Marine Turbulence*, J. C. J. Nihoul, Ed., Elsevier Oceanography Series, No. 28.

Butman, B., M. Noble and D. W. Folger, 1979. Long-term observations of bottom current and bottom sediment movement on the mid-Atlantic continental shelf. *J. Geophys. Rev.*, **84**, 1187–1205.

Cacchione, D. A., and D. E. Drake, 1982. Measurements of storm-generated bottom stresses on the continental shelf. *J. Geophys. Rev.*, **87**, 1952–1961.

Caldwell, D. R., and T. M. Chriss, 1979. The viscous sublayer at the sea floor. *Science*, **205**, 1131–1132.

Carter, G. C., and J. F. Ferrie, 1979. A coherence and cross-spectral estimation program. *Programs for Digital Signal Processing*. IEEE Press.

Champagne, F. H., C. A. Friehe, J. C. LaRue and J. C. Wyngaard, 1977. Flux measurements, flux estimation techniques and fine-scale turbulence measurements in the unstable surface layer over land. *J. Atmos. Sci.*, **34**, 515–530.

Chriss, T. M., and D. R. Caldwell, 1982. Evidence for the influence of form drag on bottom boundary layer flow. *J. Geophys. Res.*, **87**, 4148–4154.

——, D. A. Huntley and D. G. Hazen, 1983. A flexible interactive instrumentation system for the study of boundary layer turbulence (Abstract). *Eos*, **64**(45), 729.

Clarke, A. J., and K. H. Brink, 1985. The response of stratified frictional flow of shelf and slope waters to fluctuating, large-scale, low-frequency wind forcing. *J. Phys. Oceanogr.*, **15**, 439–453.

Cunningham, P. M., R. T. Guza and R. L. Lowe, 1979. Dynamic calibration of electromagnetic flowmeters. *Proc. of Oceans '79*, IEEE and Mar. Technol. Soc., 298–301.

Davidson, S., 1984. SED1D: A sediment transport model for the continental shelf. Geol. Surv. of Canada Open File Rep., Bedford Institute of Oceanography, Dartmouth, N.S., 62 pp.

Elliott, A. J., 1984. Measurements of turbulence in an abyssal boundary layer. *J. Phys. Oceanogr.*, **14**, 1779–1786.

Grant, W. D., and O. S. Madsen, 1979. Combined wave and current interaction with a rough bottom. *J. Geophys. Res.*, **84**, 1797–1808.

——, and ——, 1982. Moveable bed roughness in unsteady oscillatory flow. *J. Geophys. Res.*, **87**, 469–481.

——, and ——, 1986. The continental shelf bottom boundary layer. *Ann. Rev. Fluid Mech.*, **18**, 265–305.

——, and A. J. Williams, III, 1985. Reply to Huntley. *J. Phys. Oceanogr.*, **15**, 1219–1228.

——, —— and S. M. Glenn, 1984. Bottom stress estimates and their prediction on the Northern Californian Continental shelf during CODE-1: The importance of wave-current interaction. *J. Phys. Oceanogr.*, **14**, 507–527.

Gross, T. F., and A. R. M. Nowell, 1985. Spectral scaling in a tidal boundary layer. *J. Phys. Oceanogr.*, **15,** 496–508.

Gust, G., 1985. Comment on "Bottom stress estimates and their prediction on the Northern Californian Continental Shelf during CODE-1: The importance of wave-current interaction". *J. Phys. Oceanogr.*, **15,** 1229–1237.

Hall, R. K., 1985. Inner shelf acoustic facies and surficial sediment distribution of the Eastern Shore, Nova Scotia. Centre for Marine Geology, Tech. Rep. No. 8, Dalhousie University.

Hinze, J. O., 1975. *Turbulence,* 2d ed., McGraw-Hill, 586 pp.

Huntley, D. A., 1985. Comments on "Bottom stress estimates and their prediction on the Northern Californian Continental Shelf during CODE-1: The importance of wave-current interaction". *J. Phys. Oceanogr.*, **15,** 1217–1218.

——, 1988. A modified dissipation method for estimating seabed stresses at low Reynolds numbers, with application to wave-current boundary layer measurements. *J. Phys. Oceanogr.*, **18,** (in press).

Jonsson, I. G., 1966. Wave boundary layers and friction factors. *Proc. Tenth Coastal Engineering Conf.*, New York, Amer. Soc. Civil Engineers, Vol. 1, 127–148.

LaPierre, A. B., 1985. Modern sedimentary environments on the inner shelf, Eastern Shore, Nova Scotia. Unpublished thesis, Dept. of Geology, Dalhousie University.

Larsen, L. H., R. W. Sternberg, N. C. Shi, M. A. H. Marsden and L. Thomas, 1981. Field investigations of the threshold of grain motion by ocean waves and currents. *Mar. Geol.*, **42,** 75–104.

Lumley, J. L., and E. A. Terray, 1983. Frequency spectra of frozen turbulence in a random wave field. *J. Phys. Oceanogr.*, **13,** 2000–2007.

Smith, J. D., 1977. Modeling of sediment transport on continental shelves, *The Sea,* E. D. Goldberg and co-editors, Vol. 6, Wiley Interscience, 539–577.

Soulsby, R. L., 1980. Selecting record length and digitisation rate for near-bed turbulence measurements. *J. Phys. Oceanogr.*, **10,** 208–219.

——, 1983. The bottom boundary layer of shelf seas. *Physical Oceanography of Coastal and Shelf Seas,* Chapt. 5, B. Johns, ed., Elsevier Oceanography Series No. 35.

Tennekes, H., and J. L. Lumley, 1972. *A First Course in Turbulence,* MIT Press, 300 pp.

Wiberg, P., and J. D. Smith, 1983. A comparison of field data and theoretical models for wave-current interactions at the bed on the continental shelf. *Contin. Shelf Res.*, **2,** 126–136.

Williams, R. M., and C. A. Paulson, 1977. Microscale temperature and velocity spectra in the atmospheric boundary layer. *J. Fluid Mech.*, **83,** 547–567.

Wooding, R. A., E. F. Bradley and J. K. Marshall, 1973. Drag due to regular arrays of roughness elements of varying geometry. *Bound.-Layer Meteor.*, **5,** 285–308.

Wyngaard, J. C., and O. R. Cote, 1971. The budgets of turbulent kinetic energy and temperature variance in the atmospheric surface layer. *J. Atmos. Sci.*, **28,** 190–201.